# Towards Quantum Computing Phase Diagrams of Gauge Theories with Thermal Pure Quantum States

Zohreh Davoudi,[1,2,3,‡] Niklas Mueller,[1,4,†] and Connor Powers[1,2,*]

[1]*Maryland Center for Fundamental Physics and Department of Physics, University of Maryland, College Park, Maryland 20742, USA*
[2]*Institute for Robust Quantum Simulation, University of Maryland, College Park, Maryland 20742, USA*
[3]*Joint Center for Quantum Information and Computer Science, NIST/University of Maryland, College Park, Maryland 20742, USA*
[4]*Joint Quantum Institute, NIST/University of Maryland, College Park, Maryland 20742, USA*

(Received 28 September 2022; revised 27 February 2023; accepted 1 June 2023; published 21 August 2023)

The phase diagram of strong interactions in nature at finite temperature and chemical potential remains largely theoretically unexplored due to inadequacy of Monte-Carlo–based computational techniques in overcoming a sign problem. Quantum computing offers a sign-problem-free approach, but evaluating thermal expectation values is generally resource intensive on quantum computers. To facilitate thermodynamic studies of gauge theories, we propose a generalization of the thermal-pure-quantum-state formulation of statistical mechanics applied to constrained gauge-theory dynamics, and numerically demonstrate that the phase diagram of a simple low-dimensional gauge theory is robustly determined using this approach, including mapping a chiral phase transition in the model at finite temperature and chemical potential. Quantum algorithms, resource requirements, and algorithmic and hardware error analysis are further discussed to motivate future implementations. Thermal pure quantum states, therefore, may present a suitable candidate for efficient thermal simulations of gauge theories in the era of quantum computing.

DOI: 10.1103/PhysRevLett.131.081901

*Introduction.*—The notorious sign problem in classical Monte-Carlo–sampling techniques has slowed down progress in addressing a range of problems in the domain of nuclear and high-energy physics. These include *ab initio* nuclear many-body calculations of nucleonic matter including large-mass atomic nuclei [1–3], and lattice Quantum Chromodynamics (QCD) calculations at finite baryonic density and chemical potential [4–9], pertinent to "critical endpoint" searches in the Beam Energy Scan at the Relativistic Heavy Ion Collider [10,11], and essential in illuminating exotic QCD phases potentially present in the interior of neutron and quark stars [12–15]. Attempts to alleviate sign problems are numerous and include reweighting [16–18], Majorana [19,20] and Meron Cluster algorithms [21], stochastic quantization and complex Langevin dynamics [22–27], Taylor expansion around vanishing chemical potential [28–32], analytic continuation from imaginary chemical potential [33–35], and path deformation and complexification [36–40]. Monte-Carlo techniques can be avoided altogether using Hamiltonian-simulation methods such as Tensor Networks [41–45] and quantum-simulation-inspired algorithms [46]. Nonetheless, despite this progress, a universal approach to overcoming the sign problem in lattice-QCD calculations is not known.

Digital quantum computers, as well as analog quantum simulators, offer a sign-problem-free approach to computing ground, excited, thermal, and nonequilibrium states of quantum many-body systems including lattice gauge theories (LGTs) [47–96]. However, because quantum devices naturally implement pure states, quantum computing thermal, i.e., mixed, states is a challenging task. An obvious possibility, thermalizing a nonequilibrium state through unitary time evolution [70,97], may be costly on near-term quantum devices due to long equilibration times involved. Other methods for quantum computing thermal expectation values exist, which generally fall into two categories. One is sampling easily preparable pure states according to thermal statistics [98–104], but sampling-based techniques require larger sample sizes when the system size is increased, hence, increasing resource requirements. Another is preparing full (mixed) thermal states on the quantum computer, often relying on resource-intensive algorithms such as quantum phase estimation and incurring significant ancillary-qubit requirements [105–110]. Classical state preparation [111,112] or hybrid classical-quantum algorithms for near-term applications [99], such as those relying on variational methods [108,113–119] or utilizing Jarzynski's equality [120–122] have also been explored in recent years.

A promising near-term perspective is to resort to the thermal-pure-quantum-(TPQ-) state formulation of statistical mechanics [123–125] to obtain thermal expectation

values using only a single properly prepared pure state in the thermodynamic limit. This approach offers a promising path to simulating quantum systems at finite temperature and chemical potential on quantum computers [126,127]. Canonical TPQ states, in particular, are formed by imaginary-time evolving pure states drawn from an ensemble of Haar-random states. Thermal expectation values of mechanical observables with TPQ states converge rapidly to the values within the standard (ensemble) formulation of statistical mechanics, improving exponentially with system size. In fact, as is shown in Ref. [123], for sufficiently large systems, often a single TPQ state suffices. However, in gauge theories, local symmetries put constraints on the allowed Hilbert space so that the naïve TPQ-state approach cannot be applied. In this Letter, a protocol for explicitly constructing TPQ states in the physical subspace of gauge theories will be introduced by penalizing nonphysical components of the random pure state as they evolve in imaginary time.

By accurately obtaining, via a numerical simulation, the phase diagram of a simple gauge theory ($Z_2$ LGT in $1+1$ D with matter) at finite temperature and chemical potential, we demonstrate the utility of the TPQ-state approach in studying thermodynamics of gauge theories for the first time. Aiming at quantum-computing applications, associated quantum algorithms, quantum-resource requirements, and robustness to algorithmic and hardware errors are further studied. The results indicate that the TPQ-state approach may be a suitable candidate for efficient phase-diagram studies of QCD in the future.

*Thermal pure quantum states for gauge theories.*—Canonical TPQ states are defined as [123]

$$|\beta, N\rangle \equiv e^{-\frac{\beta}{2}H}|\psi_R\rangle, \tag{1}$$

with $\beta$ being the inverse temperature, $N$ the number of degrees of freedom of the (discrete) system, and $|\psi_R\rangle$ a Haar-random state, i.e., $\psi_R \equiv \sum_i c_i|i\rangle$, where each $c_i$ is drawn from a set of complex numbers $\{c_i\}$ on the unit sphere of the $2^N$-dimensional Hilbert space of the simulation, $\sum_i |c_i|^2 = 1$. The set $\{|i\rangle\}$ can be any arbitrary orthonormal basis that spans this Hilbert space, including simply a set of product states. TPQ states approximate thermal expectation values of "mechanical" operators, i.e., those that are low-degree polynomials of local operators, via

$$\langle O\rangle_\beta \approx \frac{\langle\!\langle \langle\beta, N|O|\beta, N\rangle \rangle\!\rangle_r}{\langle\!\langle \langle\beta, N|\beta, N\rangle \rangle\!\rangle_r}, \tag{2}$$

with exponential convergence in the system size (as well as in inverse temperature), see Supplemental Material [128] for details. While a single TPQ state suffices as $N \to \infty$, for faster convergence at finite $N$, a stochastic average over $r$ TPQ states can be performed, denoted by $\langle\!\langle \cdot \rangle\!\rangle_r$ in the formula, which, hence, reduces the error by $1/\sqrt{r}$.

In gauge theories, $|\Phi_R\rangle$ may be unphysical, in which case Eq. (1) will not reproduce physical thermal observable

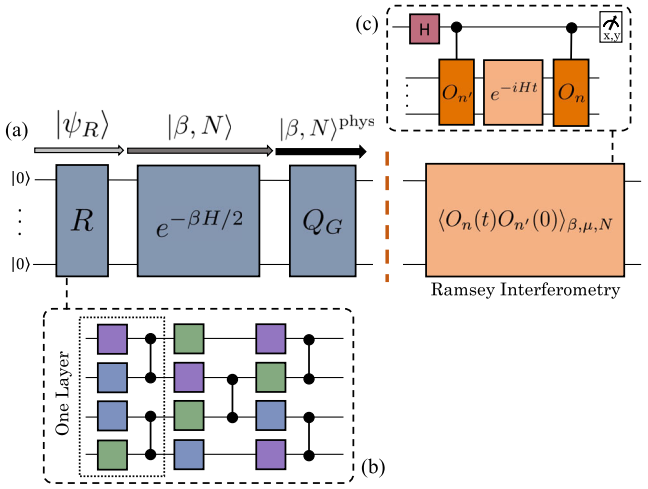


FIG. 1. (a) Schematic overview of the PTPQ-state preparation. (b) Detailed view of random state preparation sub-circuit. The colored squares in the $R$ circuit denote randomly chosen single-qubit rotations around $X$ and $Y$ axes of the Bloch sphere by angle $(\pi/2)$ and the $T$ gates. The entangling gates are controlled $Z$ rotations. The two consecutive single-qubit gates on each qubit are constrained to be different in this construction. Entangling gates in each layer only act on adjacent qubits and this pattern continues, see Ref. [141] for details. (c) Detail edview of Ramsey interferometry sub-circuit. $H$ is a Hadamard gate.

expectation values. While this issue can be avoided by eliminating the gauge-field degrees of freedom with certain boundary conditions in $1+1$ D, such a strategy is not generally applicable. Therefore, we propose "physical" thermal pure quantum (PTPQ) states

$$|\beta, N\rangle^{\text{phys}} \equiv e^{-\frac{\beta}{2}\tilde{H}}|\Psi_R\rangle, \tag{3}$$

by adding a term to the Hamiltonian, $\tilde{H} \equiv H + \sum_n f(G_n)$ where $G_n$ are Gauss's law operators at site $n$, that is $[H, G_n] = 0$. The function $f$ is chosen such that unphysical components of the state as it evolves in imaginary time are penalized in energy. Such an approach is customary in the context of enforcing Gauss's law in analog and digital quantum simulation of gauge theories and can be applied to both Abelian and non-Abelian cases [47,49,85,134–139]. It may also be used to restrict sampling-based algorithms for evaluating thermal expectation values to a smaller physical Hilbert space.

A circuit to prepare PTPQ states on quantum computers is illustrated in Fig. 1. First, a random circuit $R$, consisting of layers of single-qubit gates and entangling two-qubit gates, is used to prepare an approximate Haar-random state. Various designs are suggested for such task with studied performance [140], and we adopt the efficient implementation of Ref. [141]. This random circuit is followed by a nonunitary operator $e^{-\beta H/2}$ acting upon the resulting random state to produce a standard canonical TPQ state. Gauss's law is enforced through action with

$Q_G \equiv e^{-(\beta/2)\sum_n f(G_n)}$, the circuit implementation of which depends on the $f$ chosen, see below for the example of $Z_2$ LGT in $1+1$ D. These elements will be further studied in the following.

*Thermal chiral phase diagram of* $Z_2^{1+1}$.—The model that will be studied in the following to demonstrate the value of the TPQ-state approach in gauge theories is $Z_2$ LGT in $1+1$ D coupled to staggered fermions ($Z_2^{1+1}$). This model is sufficiently simple to allow numerical verifications on classical computers, while it still exhibits a nontrivial phase diagram which is aimed to be reproduced by quantum simulation. The Hamiltonian of the model is

$$H = \frac{1}{2a}\sum_{n=0}^{N-2}(c_n^\dagger \tilde{\sigma}_n^z c_{n+1} + \text{H.c.}) + m\sum_{n=0}^{N-1}(-1)^n c_n^\dagger c_n - \epsilon\sum_{n=0}^{N-2}\tilde{\sigma}_n^x, \tag{4}$$

where $c_n^\dagger$ ($c_n$) is the fermionic creation (annihilation) operator, and $\tilde{\sigma}_n^z$ and $\tilde{\sigma}_n^x$ are Pauli spin operators realizing the $Z_2$ link and electric-field operators, respectively. Open boundary conditions are considered throughout, and generalization to other boundary conditions is straightforward. $N$, $a$, $m$, and $\epsilon$ are fermionic lattice size, lattice spacing, fermion mass, and electric-field strength, respectively. Gauss's law operator $G_n \equiv \tilde{\sigma}_n^x \tilde{\sigma}_{n-1}^x e^{i\pi\{c_n^\dagger c_n + [(-1)^n - 1]/2\}}$ defines the physical subspace of the theory via the relation $G_n|\Psi\rangle^{\text{phys}} = |\Psi\rangle^{\text{phys}}$. For all the results shown, we set $a = 1$, $m = 1/2$, and $\epsilon/m = 1$.

Using PTQP states with $f(G_n) = \lambda(1 - G_n)$ for large $\lambda$, the chiral phase diagram of $Z_2^{1+1}$ at finite temperature $T$ and chemical potential $\mu$ can be computed. A nonzero chemical potential can be accounted for by modifying the Hamiltonian, $H \to H - \mu\sum_{n=0}^{N-1} c_n^\dagger c_n$. The order parameter to be evaluated is the chiral condensate,

$$\langle\bar{\Psi}\Psi\rangle \equiv \frac{1}{N}\left\langle\sum_{n=0}^{N-1}(-1)^n c_n^\dagger c_n\right\rangle, \tag{5}$$

with $\langle\bar{\Psi}\Psi\rangle \neq 0$ ($= 0$) in the chiral-symmetry broken (symmetric) phase. In QCD, chiral symmetry is spontaneously broken at small $T$ [142] but restored at large $T$ [143–147]. Chiral symmetry breaking is also observed in $1+1$ D Abelian gauge theories [148–150]. For $Z_2^{1+1}$ with staggered fermions, chiral symmetry restoration can be understood intuitively. At asymptotic $\mu \gg m$, $\epsilon$, the state with all fermion sites occupied dominates the thermal Gibbs ensemble and has $\langle\bar{\Psi}\Psi\rangle = 0$ according to Eq. (5), while at $T \to \infty$, the state is an equal admixture of all basis states, giving rise to a net vanishing condensate.

Figure 2 depicts the phase diagram using PTPQ states with random-circuit depth $d = 20$ and averaged over $r = 10$ PTPQ-state realizations. All results are classically computed using exact diagonalization on a system of $N = 6$ sites corresponding to 11 qubits [128]. Chiral symmetry is observed to be restored at high $T$ and $\mu$ and is broken, otherwise. Despite the small system size, the transition at $T \to 0$ is visibly discontinuous, indicating that a "true" phase transition is expected in the infinite-volume limit, while only a smooth crossover is observed at $\mu \to 0$. The top and right panels of Fig. 2 show a comparison between exact results and PTPQ states. Reasonable agreement is observed, and the accuracy is expected to improve with increasing system size, see Supplemental Material for details [128]. Furthermore, as demonstrated in the Supplemental Material [128], the standard TPQ states do not reproduce the correct phase diagram unless promoted to PTPQ states.

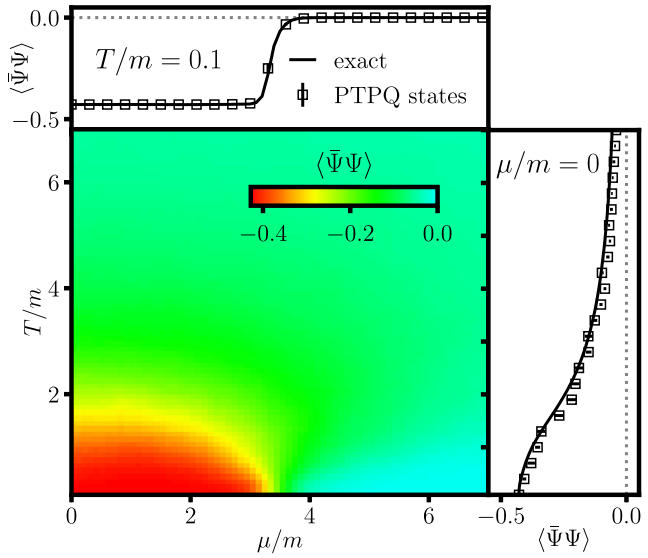


FIG. 2. Chiral phase diagram for the $Z_2$ LGT with fermions in $1+1$ D with $N = 6$ and $\lambda/m = 4$, calculated with PTPQ states with random-circuit depth $d = 20$ and averaged over $r = 10$ PTPQ-state realizations. Error bars denote statistical uncertainty from a finite PTPQ sample.

In contrast, regardless of the use of PTPQ states, detecting the confinement-deconfinement transition, where one computes nonlocal observables, e.g., string tension, is more challenging on small systems due to finite-size effects, as discussed in the Supplemental Material [128].

Thermal non-equal-time correlation functions can also be evaluated using the PTPQ-state protocol [151]. These quantities are challenging to access with classical Monte-Carlo techniques even at vanishing chemical potential. As an example, we focus on the thermal current-current correlator,

$$C_n(t) \equiv \langle[j_n(t), j_0(0)]\rangle_\beta, \tag{6}$$

relevant in the Kubo formula in linear response theory [129]. Here, $j_n(t) \equiv e^{iHt} j_n e^{-iHt}$, $j_n \equiv i/(2a)[\sigma_n^+ \tilde{\sigma}_n^z \sigma_{n+1}^- -$ H.c.] is the fermionic current operator, and $\langle\cdot\rangle_\beta$ denotes the

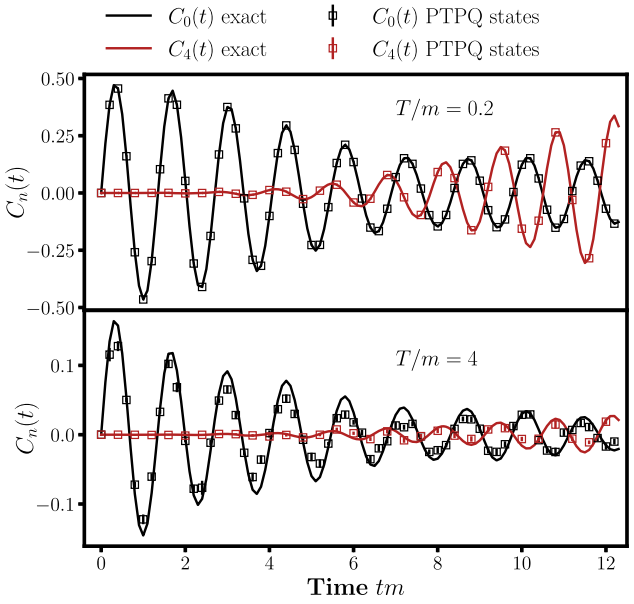


FIG. 3. Non-equal-time correlation functions $C_0(t)$ and $C_4(t)$ with $N = 6$, $\mu/m = 0.5$, and $\lambda/m = 4$. Data are shown at $T/m = 0.2$ with $r = 1$ and at $T/m = 4$ with $r = 20$.

thermal expectation value at finite $\beta$. A quantum circuit for evaluating $C_n(t)$ is presented in Fig. 1(c) and involves a standard Ramsey interferometry scheme [130,152–154], requiring an ancilla in a Hadamard superposition controlling $j_n(t)$ and $j_0(0)$, with the PTPQ-state input. The results of this procedure (classically computed) are shown in Fig. 3 for $N = 6$, $T/m = 0.2$, and $\mu/m = 0.5$. The exact results, obtained with exact diagonalization, are compared with a PTPQ computation using $r = 1$ and $r = 20$ samples for lower and higher temperatures, respectively, and good agreement is observed. Since real-time evolution is natural for a quantum computer, PTPQ states are expected to be an important tool to compute, e.g., transport quantities like conductivity or viscosity. For example, one can use Eq. (6) to compute thermal conductivity, $\sigma_{\beta,\mu} \sim \lim_{\omega\to 0}(a/\omega)\int dt\, e^{i\omega t}\sum_n C_n(t)$, which, nonetheless, requires long evolution times and large system sizes to be obtained accurately. For a nonlinear response to an external field, a framework is developed in Ref. [151], along with a set of necessary conditions, to still permit the use of a TPQ-state strategy.

*Robustness to quantum-circuit implementation errors.*— To investigate inaccuracies occurring in the quantum-circuit implementation of the PTPQ-state preparation in $Z_2^{1+1}$, we recall that this preparation consists of two parts, generation of a Haar-random state, followed by imaginary-time evolution with $H + \lambda\sum_n(1 - G_n)$.

First, by employing an exemplary current noise model, the effect of device noise in generating a Haar-random state can be investigated using the circuit described in Fig. 1(b). Shown in Fig. 4(a) is the chiral transition of an ideal device versus IBM's "Sydney" device [155] (simulator) when noise is present in the Haar-random-state preparation, while the imaginary-time evolution is performed exactly (shot noise is not considered). Data corresponds to a circuit depth of $d = 20$ and $r = 10$ PTPQ realizations for a system of $N = 6$ fermionic sites. As is seen, device errors included in current simulators have a negligible effect during this part of the algorithm. Whether features like phase transitions remain robust with respect to the actual device error will need to be tested on the available quantum hardware in future studies.

The second part of the algorithm is imaginary-time evolution. Here, an error analysis will specifically depend on the chosen implementation strategy and device. Among the common near-term approaches include the quantum imaginary time evolution (QITE) algorithm [100] and dilated operator approaches [157,158]. Both approaches may employ Trotterization for imaginary-time evolution, hence, it is beneficial to investigate the Trotterization error in the PTPQ-state preparation.

For simplicity, we consider Trotterization via a first-order product formula of the form

$$S(\beta) \equiv [S(\Delta\beta)]^{N_T} \equiv \left[\prod_{\gamma=1}^{\Gamma} e^{-H_\gamma \Delta\beta}\right]^{N_T}, \tag{7}$$

with $\Delta\beta \equiv \beta/(2N_T)$, where $H = \sum_{\gamma=1}^{\Gamma} H_\gamma$ with $H_\gamma$ being each noncommuting term in the $Z_2^{1+1}$ Hamiltonian in Eq. (4) plus the chemical-potential contribution, after Jordan-Wigner transforming fermionic into spin degrees of freedom. Note that implementing $Q_G$ does not introduce any Trotter error as $[H_n, Q_G] = 0$. The Trotter-step ($N_T$) dependence of the chiral condensate $\langle\bar{\Psi}\Psi\rangle$ as a function of chemical potential $\mu$ at a relatively long imaginary time corresponding to temperature $T/m = 0.1$ is plotted in Fig. 4(b). As is seen, with a small number of steps $N_T = 10$ ($\Delta\beta = 1$), the chiral phase transition is reproduced qualitatively. To achieve percent-level agreement, $N_T \gtrsim 100$ is required corresponding to step sizes $\Delta\beta \lesssim 0.1$. This suggests that, despite large Trotter errors, qualitative features of the phase diagram, such as phase transitions, can still be accessible.

An analytic bound for the additive Trotter error $\mathcal{A}(\Delta\beta) \equiv S(\Delta\beta) - e^{-\Delta\beta H}$ has been obtained in Ref. [156], which, for the first-order formula, reads

$$\|\mathcal{A}(\Delta\beta)\| = \mathcal{O}\left(\tilde{\alpha}_{\text{comm}}(\Delta\beta)^2 e^{4\Delta\beta\sum_{\gamma=1}^{\Gamma}\|H_\gamma\|}\right). \tag{8}$$

Here, $\tilde{\alpha}_{\text{comm}} \equiv \sum_{\gamma_1,\gamma_2=1}^{\Gamma}\|[H_{\gamma_2}, H_{\gamma_1}]\|$ and $\|\cdot\|$ is the spectral norm. In the Supplemental Material [128], we show that when the Hermiticity of the Hamiltonian is taken into account, a new bound can be obtained,

$$\|\mathcal{A}(\Delta\beta)\| = \mathcal{O}\left(\tilde{\alpha}_{\text{comm}}(\Delta\beta)^2 e^{-\Delta\beta\sum_{\gamma=1}^{\Gamma} E_0^{(H_\gamma)}}\right). \tag{9}$$

Here, $E_0^{(H_\gamma)}$ is the lowest eigenvalue of each Hamiltonian term $H_\gamma$. $H_\gamma$ could be a single term or a collection of

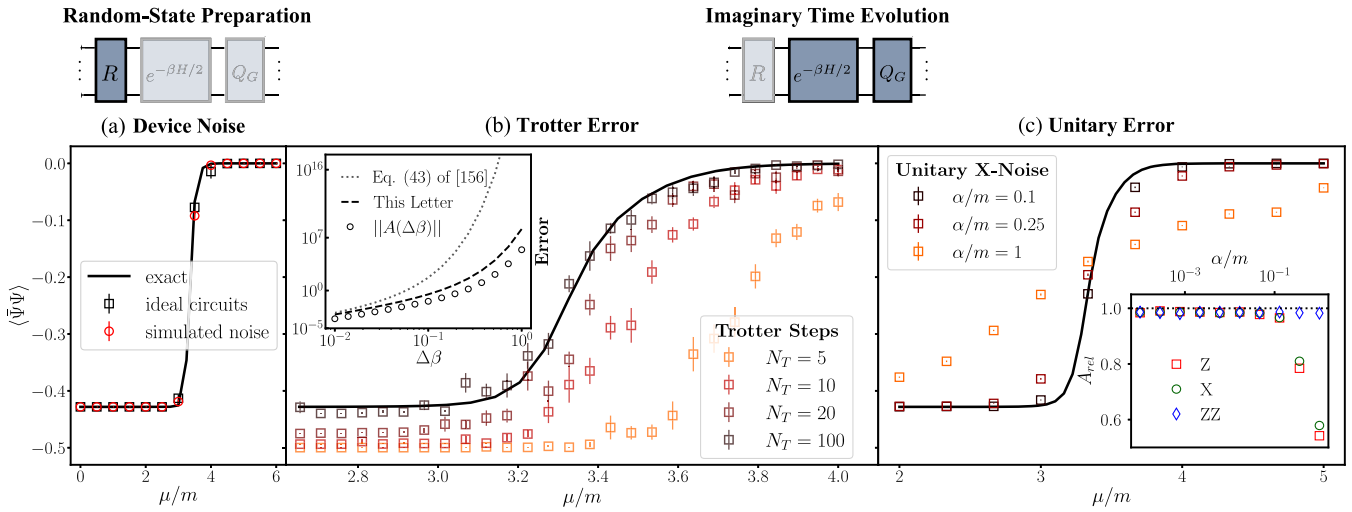


FIG. 4. (a) Chiral condensate $\langle\bar{\Psi}\Psi\rangle$ as a function of $\mu/m$, including simulated device noise [155] on the Haar-random state-preparation circuit shown in Fig. 1(b). (b) Trotterization error in evaluating $\langle\bar{\Psi}\Psi\rangle$ as a function of $\mu/m$ for various numbers of Trotter steps $N_T$. Inset: The first-order product-formula additive Trotter error bound from Eq. (43) of Ref. [156] [Eq. (8) of this Letter] and the new bound of this Letter in Eq. (9) as a function of $\Delta\beta$ for $N = 6$ at $\mu/m = 4$. Explicitly calculated additive Trotter error $\|\mathcal{A}(\Delta\beta)\|$ is plotted for comparison. (c) Unitary errors in $\langle\bar{\Psi}\Psi\rangle$ as a function of $\mu/m$ calculated with PTPQ states with introduced unitary $X$ errors at various relative Hamiltonian error strengths $\alpha/m$. Inset: Relative accuracy $A_{\text{rel}}$ as a function of relative Hamiltonian error-term strength $\alpha/m$ at $\mu/m = 3$ when various types of unitary error are added to the imaginary-time evolution. All results are obtained for $d = 20$, $r = 10$, $\lambda/m = 8$, $T/m = 0.1$, and averaged over results from 50 randomly generated error terms at each value of $\alpha/m$.

commuting terms, whose lowest eigenvalue can be classically evaluated efficiently. The inset of Fig. 4(b) shows the additive Trotter error as a function of $\Delta\beta$ using both bounds in Eqs. (8) and (9), along with the numerically determined $\|\mathcal{A}(\Delta\beta)\|$. The Hamiltonian is split according to $H = H_e + H_o + H_D$, where $H_{e/o} \equiv 1/(2a)\sum_{n\in\text{even/odd}}(c_n^\dagger\tilde{\sigma}_n^z c_{n+1} + \text{H.c.})$ and $H_D \equiv m\sum_n(-1)^n c_n^\dagger c_n - \epsilon\sum_n\tilde{\sigma}_n^x - \mu\sum_n c_n^\dagger c_n$. As can be seen, compared with Eq. (8), the new bound in Eq. (9) is closer to the numerically determined error. We should note that an improved version of the bound in Eq. (14) of Ref. [156]: $\|\mathcal{A}(\Delta\beta)\| = \mathcal{O}(\tilde{\alpha}_{\text{comm}}(\Delta\beta)^2\times e^{\Delta\beta\sum_{\gamma=1}^{\Gamma}\|H_\gamma\|})$, on the other hand, is equal to our bound in Eq. (9) since for this model, $\|H\| = |E_0|$. The result in Eq. (9), however, provides a tighter bound when $\|H\| > |E_0|$, for example in bosonic quantum field theories with an unbounded spectrum.

The influence of device errors on the imaginary-time evolution, through imperfect gates and decoherence, is hardware and algorithm specific and, thus, difficult to estimate. Nonetheless, one can consider a device-independent approach, in which the errors can be parametrized as imaginary-time evolution under an effective Hamiltonian [159] $H' = \tilde{H} + H_{\text{err}}^\alpha$, with $H_{\text{err}}^\alpha$ representing 1- or 2-local errors with randomized weights bounded by $\alpha$. Because both fermion (via a Jordan-Wigner transformation) and gauge variables are spin operators, they will be denoted from now on with the same symbol $\sigma_n^{x/z}, \tilde{\sigma}_n^{x/z} \to \sigma_l^{x/z}$, where $l$ denotes sites in a chain of length $2N-1$, and even (odd) sites labeling fermions (gauge fields). Motivated by the common bit flip, phase flip, and crosstalk errors in current hardware, we choose $H_{\text{err}} = \sum_{l=0}^{2N-1} K_l^\alpha\sigma_l$, where $\sigma_l \in \{\sigma_l^x, \sigma_l^z, \sigma_l^z\sigma_{l+1}^z\}$, and $K_l^\alpha$ is sampled uniformly from $[-\alpha, \alpha]$. Denoting $\langle\bar{\Psi}\Psi\rangle^{\text{PTPQ}}(\alpha)$ the chiral condensate calculated with the PTPQ states under such a noise model, a relative accuracy can be defined as

$$A_{\text{rel}} \equiv 1 - \frac{|\langle\bar{\Psi}\Psi\rangle^{\text{PTPQ}}(\alpha) - \langle\bar{\Psi}\Psi\rangle|}{|\langle\bar{\Psi}\Psi\rangle|}. \tag{10}$$

The chiral condensate under this noise model is plotted in Fig. 4(c) as a function of chemical potential, at $T/m = 0.1$ for $\alpha/m = 0.1, 0.25, 1$, with exact values displayed for reference. For $\sigma_l^x$ errors, PTPQ states are still able to capture phase transitions for $\alpha/m = 0.1$, but this ability decays as $\alpha/m \to 1$, as the relative accuracy near the transition quickly drops to $\sim$45%. Furthermore, the inset of Fig. 4(c) shows $A_{\text{rel}}$ for $\mu/m = 1.5$ as a function of $\alpha/m$.

A strong difference is observed between $\sigma_l^z$ and $\sigma_l^x$ errors versus $\sigma_l^z\sigma_{l+1}^z$ errors. $\tilde{\sigma}_n^x$ and $\sigma_n^z$ are both gauge invariant, so the introduced $X$-type and $Z$-type noise only violate Gauss's law on half of the qubits. Conversely, $ZZ$-type noise always violates Gauss's law since each term acts on one link and one site. Since the penalty term $Q_G$ effectively protects against Gauss's-law-violating errors, PTPQ states are seen to be more robust to the latter. In the Supplemental Material [128], we discuss the relation between the link-operator convention and the unitary-noise mitigation. Finally, we point out that an approach which treats the error

terms as truly "unitary," that is by replacing $K_l^a \to iK_l^a$, has also been tried numerically and resulted in no qualitative difference compared to the presented scheme.

*Scaling and resource requirements.*—While an exact preparation of Haar-random state has a time complexity that scales exponentially in the system size, pseudo-Haar-random states that are sufficient for most applications can be prepared in polynomial time, as has been established in Refs. [141,160–162]. For example, the (pseudo-) random-state preparation circuit for PTPQ states in this Letter requires only $\mathcal{O}(Nd)$ two-qubit entangling gates, where $N$ is the number of qubits and $d$ is number of layers. In practice, $d \simeq 20$ is seen to be sufficient in the examples of this Letter. In general, the required $d$ for given precision depends on the system size, but the scaling is observed to be sublinear [141,162,163].

To cost the imaginary-time evolution, we consider the QITE algorithm [100] because of its prominence among near-term approaches. The QITE algorithm consists of Trotterizing imaginary-time evolution, e.g., Eq. (7), and it proceeds to find, using classical processing or variationally, a unitary operator $e^{-i\Delta\beta A_\gamma}$ that approximates the nonunitary operator $e^{-H_\gamma\Delta\beta}$, such that for given intermediate state $|\Phi\rangle$ in the Trotter sequence, $e^{-i\Delta\beta A_\gamma}|\Phi\rangle \approx e^{-H_\gamma\Delta\beta}|\Phi\rangle/\mathcal{N}_\beta$, where $\mathcal{N}_\beta \equiv \langle\Phi|e^{-2H_\gamma\Delta\beta}|\Phi\rangle$. Note that for PTPQ-state preparation, $\mathcal{Q}_G$ does not need to be Trotterized and can be performed in a single QITE step for time duration $\beta$.

Following this protocol, one incurs two types of errors: the Trotter error $\varepsilon_T \geq \|A(\Delta\beta)\|$, discussed in the previous section, and the intrinsic QITE error $\varepsilon_Q$ from approximating a nonunitary evolution with a unitary evolution after $N_T$ applications. Here, $A_\gamma$ acts on $N_q$ qubits. Increasing $N_q$ reduces $\varepsilon_Q$ but increases the $A_\gamma$ circuit cost, i.e., the total algorithm runtime of the QITE algorithm is $\Gamma N_T e^{\mathcal{O}(N_q)}$ [100,128]. To estimate this dependence, assume $N_T \geq \beta\eta$ where $\|H_\gamma\| \leq \eta$ is a bound on the operator norm of $H_\gamma$. Then $N_q = \mathcal{O}(2k\mathcal{C}\ln[2\sqrt{2}\Gamma N_T\varepsilon_Q^{-1}])$, with $k$ the locality of the Hamiltonian and $\mathcal{C}$ the typical correlation length of the state which is acted upon. The Trotter-step dependence can be exchanged with Trotter error $\varepsilon_T$ using Eq. (8). Further details on the algorithmic scaling is provided in the Supplemental Material [128].

Note that, in essence, the QITE circuit complexity is exponential in the correlation length $\mathcal{C}$. While the PTPQ algorithm starts from an infinite-temperature state, where $\mathcal{C} = 0$, this will become prohibitive at a phase transition (of an infinite system), thus, highlighting the importance of developing efficient far-term nonunitary evolution schemes. Variational methods and near-term efficient implementation of dilated-operator and block-encoding algorithms have been recently explored, see, e.g., Refs. [164–167].

*Conclusions.*—Physical thermal pure quantum states, introduced in this Letter as an extension of (canonical) thermal pure quantum states, present a valuable method for quantum computing thermal phase diagram and thermal non-equal-time correlation functions in strongly interacting gauge theories. Via the example of a $1+1$ dimensional $Z_2$ lattice gauge theory coupled to staggered fermions on a small lattice, PTPQ states are shown numerically to reproduce the phase diagram very accurately over all values of temperature and chemical potential, including a chiral phase transition, with favorable resource requirements. Phase transitions without a local order parameter, such as the (de-)confinement transition present in this model, are strongly finite-size dependent and will be accessible to future quantum computers. Similarly, thermal non-equal-time correlation functions, important for obtaining transport properties of the quark-gluon plasma in ultrarelativistic heavy ion collisions [168] can be accessed using algorithms of this Letter on the upcoming quantum-computing devices.

Z. D. and N. M. acknowledge funding by the U.S. Department of Energy's Office of Science, Office of Nuclear Physics via the program on Quantum Horizons: QIS Research and Innovation for Nuclear Science under Award No. DE-SC0021143. Z. D and C. P. acknowledge funding by the U.S. Department of Energy's Office of Science, Office of Advanced Scientific Computing Research, Accelerated Research in Quantum Computing Program Award No. DE-SC0020312. C. P. was further supported by the National Science Foundation under Quantum Leap Challenge Institute Grant No. OMA-2120757.

*Corresponding author.
cdpowers@umd.edu
†niklasmu@uw.edu
Present address: InQubator for Quantum Simulation (IQuS), Department of Physics, University of Washington, Seattle, Washington 98195, USA.
‡davoudi@umd.edu

[1] J. Carlson, S. Gandolfi, F. Pederiva, S. C. Pieper, R. Schiavilla, K. E. Schmidt, and R. B. Wiringa, Quantum Monte Carlo methods for nuclear physics, Rev. Mod. Phys. **87**, 1067 (2015).
[2] T. A. Lähde, T. Luu, D. Lee, U.-G. Meißner, E. Epelbaum, H. Krebs, and G. Rupak, Nuclear lattice simulations using symmetry-sign extrapolation, Eur. Phys. J. A **51**, 92 (2015).
[3] D. Roscher, J. Braun, J.-W. Chen, and J. E. Drut, Fermi gases with imaginary mass imbalance and the sign problem in Monte-Carlo calculations, J. Phys. G **41**, 055110 (2014).
[4] P. De Forcrand, Simulating QCD at finite density, Proc. Sci. LAT2009 (**2009**) 010.
[5] H.-T. Ding, F. Karsch, and S. Mukherjee, Thermodynamics of strong-interaction matter from lattice QCD, Int. J. Mod. Phys. E **24**, 1530007 (2015).
[6] R. Soltz, C. DeTar, F. Karsch, S. Mukherjee, and P. Vranas, Lattice QCD thermodynamics with physical quark masses, Annu. Rev. Nucl. Part. Sci. **65**, 379 (2015).

[7] G. Aarts, Introductory lectures on lattice QCD at nonzero baryon number, J. Phys. Conf. Ser. **706**, 022004 (2016).

[8] C. Ratti, Lattice QCD and heavy ion collisions: A review of recent progress, Rep. Prog. Phys. **81**, 084301 (2018).

[9] A. Bazavov, F. Karsch, S. Mukherjee, and P. Petreczky, Hot-dense lattice QCD, Eur. Phys. J. A **55**, 194 (2019).

[10] D. Cebra *et al.* (STAR Collaboration), Studying the phase diagram on QCD matter at RHIC, in *APS Division of Nuclear Physics Meeting Abstracts* (American Physical Society, College Park, Maryland, 2014), Vol. 2014, pp. FJ–001.

[11] H. Petersen, Beam energy scan theory: Status and open questions, Nucl. Phys. **A967**, 145 (2017).

[12] J. B. Kogut and M. A. Stephanov, *The Phases of Quantum Chromodynamics: From Confinement to Extreme Environments* (Cambridge University Press, Cambridge, England, 2004), Vol. 21.

[13] M. Stephanov, QCD phase diagram: An overview, Proc. Sci. LAT2006 (**2006**) 024.

[14] K. Fukushima and T. Hatsuda, The phase diagram of dense QCD, Rep. Prog. Phys. **74**, 014001 (2010).

[15] J. N. Guenther, Overview of the QCD phase diagram, Eur. Phys. J. A **57**, 136 (2021).

[16] T. D. Kieu and C. J. Griffin, Monte Carlo simulations with indefinite and complex-valued measures, Phys. Rev. E **49**, 3855 (1994).

[17] Z. Fodor and S. D. Katz, A new method to study lattice QCD at finite temperature and chemical potential, Phys. Lett. B **534**, 87 (2002).

[18] Z. Fodor and S. D. Katz, Lattice determination of the critical point of QCD at finite $T$ and $\mu$, J. High Energy Phys. 03 (2002) 014.

[19] Z.-X. Li, Y.-F. Jiang, and H. Yao, Solving the fermion sign problem in quantum Monte Carlo simulations by Majorana representation, Phys. Rev. B **91**, 241117(R) (2015).

[20] Z.-X. Li, Y.-F. Jiang, and H. Yao, Majorana-Time-Reversal Symmetries: A Fundamental Principle for Sign-Problem-Free Quantum Monte Carlo Simulations, Phys. Rev. Lett. **117**, 267002 (2016).

[21] S. Chandrasekharan and U.-J. Wiese, Meron-Cluster Solution of Fermion Sign Problems, Phys. Rev. Lett. **83**, 3116 (1999).

[22] G. Aarts and I.-O. Stamatescu, Stochastic quantization at finite chemical potential, J. High Energy Phys. 09 (2008) 018.

[23] G. Aarts, Can Stochastic Quantization Evade the Sign Problem? The Relativistic Bose Gas at Finite Chemical Potential, Phys. Rev. Lett. **102**, 131601 (2009).

[24] G. Aarts, Complex Langevin dynamics and other approaches at finite chemical potential, Proc. Sci. LATTICE2012 (**2012**) 017.

[25] G. Aarts, E. Seiler, and I.-O. Stamatescu, Complex Langevin method: When can it be trusted?, Phys. Rev. D **81**, 054508 (2010).

[26] J. B. Kogut and D. K. Sinclair, Applying complex Langevin simulations to lattice QCD at finite density, Phys. Rev. D **100**, 054512 (2019).

[27] C. E. Berger, L. Rammelmüller, A. C. Loheac, F. Ehmann, J. Braun, and J. E. Drut, Complex Langevin and other approaches to the sign problem in quantum many-body physics, Phys. Rep. **892**, 1 (2021).

[28] P. De Forcrand and O. Philipsen, The QCD phase diagram for small densities from imaginary chemical potential, Nucl. Phys. **B642**, 290 (2002).

[29] S. Ejiri, C. R. Allton, S. J. Hands, O. Kaczmarek, F. Karsch, E. Laermann, and C. Schmidt, Study of QCD thermodynamics at finite density by Taylor expansion, Prog. Theor. Phys. Suppl. **153**, 118 (2004).

[30] F. Karsch, B.-J. Schaefer, M. Wagner, and J. Wambach, Towards finite density QCD with Taylor expansions, Phys. Lett. B **698**, 256 (2011).

[31] C. Bonati, M. D'Elia, F. Negro, F. Sanfilippo, and K. Zambello, Curvature of the pseudocritical line in QCD: Taylor expansion matches analytic continuation, Phys. Rev. D **98**, 054510 (2018).

[32] A. Bazavov, H.-T. Ding, P. Hegde, O. Kaczmarek, F. Karsch, N. Karthik, E. Laermann, A. Lahiri, R. Larsen, S.-T. Li *et al.*, Chiral crossover in QCD at zero and non-zero chemical potentials, Phys. Lett. B **795**, 15 (2019).

[33] R. Bellwied, S. Borsányi, Z. Fodor, J. Günther, S. Katz, C. Ratti, and K. Szabo, The QCD phase diagram from analytic continuation, Phys. Lett. B **751**, 559 (2015).

[34] C. Bonati, M. D'Elia, M. Mariti, M. Mesiti, F. Negro, and F. Sanfilippo, Curvature of the chiral pseudocritical line in QCD: Continuum extrapolated results, Phys. Rev. D **92**, 054503 (2015).

[35] S. Borsanyi, Z. Fodor, J. N. Guenther, R. Kara, S. D. Katz, P. Parotto, A. Pasztor, C. Ratti, and K. K. Szabó, QCD Crossover at Finite Chemical Potential from Lattice Simulations, Phys. Rev. Lett. **125**, 052001 (2020).

[36] M. Cristoforetti, F. Di Renzo, L. Scorzato (AuroraScience Collaboration), New approach to the sign problem in quantum field theories: High density QCD on a Lefschetz thimble, Phys. Rev. D **86**, 074506 (2012).

[37] M. Cristoforetti, F. Di Renzo, A. Mukherjee, and L. Scorzato, Monte Carlo simulations on the Lefschetz thimble: Taming the sign problem, Phys. Rev. D **88**, 051501(R) (2013).

[38] G. Başar, Going with the flow: A new solution to the sign problem, Nucl. Phys. **A967**, 852 (2017).

[39] A. Alexandru, G. Başar, P. F. Bedaque, and N. C. Warrington, Tempered transitions between thimbles, Phys. Rev. D **96**, 034513 (2017).

[40] A. Alexandru, G. Başar, P. F. Bedaque, and N. C. Warrington, Complex paths around the sign problem, Rev. Mod. Phys. **94**, 015006 (2022).

[41] M. C. Bañuls, K. Cichy, J. I. Cirac, K. Jansen, and H. Saito, Thermal evolution of the Schwinger model with matrix product operators, Phys. Rev. D **92**, 034519 (2015).

[42] M. C. Banuls, K. Cichy, K. Jansen, and H. Saito, Chiral condensate in the Schwinger model with matrix product operators, Phys. Rev. D **93**, 094512 (2016).

[43] M. C. Bañuls, K. Cichy, J. I. Cirac, K. Jansen, and S. Kühn, Density Induced Phase Transitions in the Schwinger Model: A Study with Matrix Product States, Phys. Rev. Lett. **118**, 071601 (2017).

[44] B. Buyens, F. Verstraete, and K. Van Acoleyen, Hamiltonian simulation of the Schwinger model at finite temperature, Phys. Rev. D **94**, 085018 (2016).
[45] G. Magnifico, T. Felser, P. Silvi, and S. Montangero, Lattice quantum electrodynamics in $(3+1)$-dimensions at finite density with tensor networks, Nat. Commun. **12**, 3600 (2021).
[46] A. M. Czajka, Z.-B. Kang, H. Ma, and F. Zhao, Quantum simulation of chiral phase transitions, J. High Energy Phys. 08 (2022) 209.
[47] D. Banerjee, M. Dalmonte, M. Müller, E. Rico, P. Stebler, U.-J. Wiese, and P. Zoller, Atomic Quantum Simulation of Dynamical Gauge Fields Coupled to Fermionic Matter: From String Breaking to Evolution After a Quench, Phys. Rev. Lett. **109**, 175302 (2012).
[48] E. Zohar, J. I. Cirac, and B. Reznik, Simulating $(2+1)$-Dimensional Lattice QED with Dynamical Matter Using Ultracold Atoms, Phys. Rev. Lett. **110**, 055302 (2013).
[49] E. Zohar, J. I. Cirac, and B. Reznik, Quantum simulations of lattice gauge theories using ultracold atoms in optical lattices, Rep. Prog. Phys. **79**, 014401 (2015).
[50] J. Mildenberger, W. Mruczkiewicz, J. C. Halimeh, Z. Jiang, and P. Hauke, Probing confinement in a $Z_2$ lattice gauge theory on a quantum computer, arXiv:2203.08905.
[51] D. Yang, G. S. Giri, M. Johanning, C. Wunderlich, P. Zoller, and P. Hauke, Analog quantum simulation of $(1+1)$-dimensional lattice QED with trapped ions, Phys. Rev. A **94**, 052321 (2016).
[52] T. V. Zache, F. Hebenstreit, F. Jendrzejewski, M. Oberthaler, J. Berges, and P. Hauke, Quantum simulation of lattice gauge theories using Wilson fermions, Quantum Sci. Technol. **3**, 034010 (2018).
[53] Z. Davoudi, M. Hafezi, C. Monroe, G. Pagano, A. Seif, and A. Shaw, Towards analog quantum simulations of lattice gauge theories with trapped ions, Phys. Rev. Res. **2**, 023015 (2020).
[54] F. M. Surace, P. P. Mazza, G. Giudici, A. Lerose, A. Gambassi, and M. Dalmonte, Lattice Gauge Theories and String Dynamics in Rydberg Atom Quantum Simulators, Phys. Rev. X **10**, 021041 (2020).
[55] D. Luo, J. Shen, M. Highman, B. K. Clark, B. DeMarco, A. X. El-Khadra, and B. Gadway, Framework for simulating gauge theories with dipolar spin systems, Phys. Rev. A **102**, 032617 (2020).
[56] B. Andrade, Z. Davoudi, T. Graß, M. Hafezi, G. Pagano, and A. Seif, Engineering an effective three-spin Hamiltonian in trapped-ion systems for applications in quantum simulation, Quantum Sci. Technol. **7**, 034001 (2022).
[57] N. Klco, E. F. Dumitrescu, A. J. McCaskey, T. D. Morris, R. C. Pooser, M. Sanz, E. Solano, P. Lougovski, and M. J. Savage, Quantum-classical computation of Schwinger model dynamics using quantum computers, Phys. Rev. A **98**, 032331 (2018).
[58] H.-H. Lu, N. Klco, J. M. Lukens, T. D. Morris, A. Bansal, A. Ekström, G. Hagen, T. Papenbrock, A. M. Weiner, M. J. Savage, and P. Lougovski, Simulations of subatomic many-body physics on a quantum frequency processor, Phys. Rev. A **100**, 012320 (2019).
[59] L. Barbiero, C. Schweizer, M. Aidelsburger, E. Demler, N. Goldman, and F. Grusdt, Coupling ultracold matter to dynamical gauge fields in optical lattices: From flux attachment to $\mathbb{Z}_2$ lattice gauge theories, Sci. Adv. **5**, eaav7444 (2019).
[60] B. Chakraborty, M. Honda, T. Izubuchi, Y. Kikuchi, and A. Tomiya, Classically emulated digital quantum simulation of the Schwinger model with a topological term via adiabatic state preparation, Phys. Rev. D **105**, 094503 (2022).
[61] A. F. Shaw, P. Lougovski, J. R. Stryker, and N. Wiebe, Quantum algorithms for simulating the lattice Schwinger model, Quantum **4**, 306 (2020).
[62] J. R. Stryker, Shearing approach to gauge invariant Trotterization, arXiv:2105.11548.
[63] Z. Davoudi, N. M. Linke, and G. Pagano, Toward simulating quantum field theories with controlled phonon-ion dynamics: A hybrid analog-digital approach, Phys. Rev. Res. **3**, 043072 (2021).
[64] L. Homeier, C. Schweizer, M. Aidelsburger, A. Fedorov, and F. Grusdt, $\mathbb{Z}_2$ lattice gauge theories and Kitaev's toric code: A scheme for analog quantum simulation, Phys. Rev. B **104**, 085138 (2021).
[65] G. Pederiva, A. Bazavov, B. Henke, L. Hostetler, D. Lee, H.-W. Lin, and A. Shindler, Quantum state preparation for the Schwinger model, in *Proceedings of the 38th International Symposium on Lattice Field Theory* (International School for Advanced Studies, Trieste, 2021).
[66] A. Rajput, A. Roggero, and N. Wiebe, Hybridized methods for quantum simulation in the interaction picture, Quantum **6**, 780 (2022).
[67] E. A. Martinez, C. A. Muschik, P. Schindler, D. Nigg, A. Erhard, M. Heyl, P. Hauke, M. Dalmonte, T. Monz, P. Zoller *et al.*, Real-time dynamics of lattice gauge theories with a few-qubit quantum computer, Nature (London) **534**, 516 (2016).
[68] N. H. Nguyen, M. C. Tran, Y. Zhu, A. M. Green, C. H. Alderete, Z. Davoudi, and N. M. Linke, Digital quantum simulation of the Schwinger model and symmetry protection with trapped ions, PRX Quantum **3**, 020324 (2022).
[69] A. Mil, T. V. Zache, A. Hegde, A. Xia, R. P. Bhatt, M. K. Oberthaler, P. Hauke, J. Berges, and F. Jendrzejewski, A scalable realization of local U (1) gauge invariance in cold atomic mixtures, Science **367**, 1128 (2020).
[70] Z.-Y. Zhou, G.-X. Su, J. C. Halimeh, R. Ott, H. Sun, P. Hauke, B. Yang, Z.-S. Yuan, J. Berges, and J.-W. Pan, Thermalization dynamics of a gauge theory on a quantum simulator, Science **377**, 311 (2022).
[71] T. Byrnes and Y. Yamamoto, Simulating lattice gauge theories on a quantum computer, Phys. Rev. A **73**, 022328 (2006).
[72] E. Zohar, J. I. Cirac, and B. Reznik, Quantum simulations of gauge theories with ultracold atoms: Local gauge invariance from angular-momentum conservation, Phys. Rev. A **88**, 023617 (2013).
[73] E. Zohar, J. I. Cirac, and B. Reznik, Cold-Atom Quantum Simulator for SU(2) Yang-Mills Lattice Gauge Theory, Phys. Rev. Lett. **110**, 125304 (2013).
[74] L. Tagliacozzo, A. Celi, P. Orland, M. Mitchell, and M. Lewenstein, Simulation of non-Abelian gauge theories with optical lattices, Nat. Commun. **4**, 2615 (2013).

[75] W. A. de Jong, K. Lee, J. Mulligan, M. Płoskoń, F. Ringer, and X. Yao, Quantum simulation of nonequilibrium dynamics and thermalization in the Schwinger model, Phys. Rev. D **106**, 054508 (2022).

[76] N. Klco, M. J. Savage, and J. R. Stryker, SU(2) non-Abelian gauge field theory in one dimension on digital quantum computers, Phys. Rev. D **101**, 074512 (2020).

[77] Y. Y. Atas, J. Zhang, R. Lewis, A. Jahanpour, J. F. Haase, and C. A. Muschik, SU(2) hadrons on a quantum computer via a variational approach, Nat. Commun. **12**, 6499 (2021).

[78] S. Rahman, R. Lewis, E. Mendicelli, and S. Powell, SU(2) lattice gauge theory on a quantum annealer, Phys. Rev. D **104**, 034501 (2021).

[79] J. F. Haase, L. Dellantonio, A. Celi, D. Paulson, A. Kan, K. Jansen, and C. A. Muschik, A resource efficient approach for quantum and classical simulations of gauge theories in particle physics, Quantum **5**, 393 (2021).

[80] A. Kan and Y. Nam, Lattice quantum chromodynamics and electrodynamics on a universal quantum computer, arXiv:2107.12769.

[81] Z. Davoudi, I. Raychowdhury, and A. Shaw, Search for efficient formulations for Hamiltonian simulation of non-Abelian lattice gauge theories, Phys. Rev. D **104**, 074505 (2021).

[82] A. Ciavarella, N. Klco, and M. J. Savage, Trailhead for quantum simulation of SU(3) Yang-Mills lattice gauge theory in the local multiplet basis, Phys. Rev. D **103**, 094501 (2021).

[83] M. S. Alam, S. Hadfield, H. Lamm, and A. C. Y. Li, Primitive quantum gates for dihedral gauge theories, Phys. Rev. D **105**, 114501 (2022).

[84] D. Paulson, L. Dellantonio, J. F. Haase, A. Celi, A. Kan, A. Jena, C. Kokail, R. van Bijnen, K. Jansen, P. Zoller, and C. A. Muschik, Simulating 2D effects in lattice gauge theories on a quantum computer, PRX Quantum **2**, 030334 (2021).

[85] J. C. Halimeh, H. Lang, and P. Hauke, Gauge protection in non-Abelian lattice gauge theories, New J. Phys. **24**, 033015 (2022).

[86] A. N. Ciavarella and I. A. Chernyshev, Preparation of the SU(3) lattice Yang-Mills vacuum with variational quantum methods, Phys. Rev. D **105**, 074504 (2022).

[87] H. Lamm, S. Lawrence, Y. Yamauchi (NuQS Collaboration), General methods for digital quantum simulation of gauge theories, Phys. Rev. D **100**, 034518 (2019).

[88] T. D. Cohen, H. Lamm, S. Lawrence, Y. Yamauchi *et al.* (NuQS Collaboration), Quantum algorithms for transport coefficients in gauge theories, Phys. Rev. D **104**, 094514 (2021).

[89] D. González-Cuadra, T. V. Zache, J. Carrasco, B. Kraus, and P. Zoller, Hardware Efficient Quantum Simulation of Non-Abelian Gauge Theories with Qudits on Rydberg Platforms, Phys. Rev. Lett. **129**, 160501 (2022).

[90] Y. Y. Atas, J. F. Haase, J. Zhang, V. Wei, S. M.-L. Pfaendler, R. Lewis, and C. A. Muschik, Simulating one-dimensional quantum chromodynamics on a quantum computer: Real-time evolutions of tetra- and pentaquarks, arXiv:2207.03473.

[91] R. C. Farrell, I. A. Chernyshev, S. J. M. Powell, N. A. Zemlevskiy, M. Illa, and M. J. Savage, Preparations for quantum simulations of quantum chromodynamics in $1+1$ dimensions. I. Axial gauge, Phys. Rev. D **107**, 054512 (2023).

[92] E. M. Murairi, M. J. Cervia, H. Kumar, P. F. Bedaque, and A. Alexandru, How many quantum gates do gauge theories require?, Phys. Rev. D **106**, 094504 (2022).

[93] G. Clemente, A. Crippa, and K. Jansen, Strategies for the determination of the running coupling of $(2+1)$-dimensional QED with quantum computing, Phys. Rev. D **106**, 114511 (2022).

[94] M. C. Banuls, R. Blatt, J. Catani, A. Celi, J. I. Cirac, M. Dalmonte, L. Fallani, K. Jansen, M. Lewenstein, S. Montangero *et al.*, Simulating lattice gauge theories within quantum technologies, Eur. Phys. J. D **74**, 165 (2020).

[95] N. Klco, A. Roggero, and M. J. Savage, Standard model physics and the digital quantum revolution: Thoughts about the interface, Rep. Prog. Phys. **85**, 064301 (2022).

[96] C. W. Bauer, Z. Davoudi, A. B. Balantekin, T. Bhattacharya, M. Carena, W. A. de Jong, P. Draper, A. El-Khadra, N. Gemelke, M. Hanada, D. Kharzeev *et al.*, Quantum simulation for high-energy physics, PRX Quantum **4**, 027001 (2023).

[97] N. Mueller, T. V. Zache, and R. Ott, Thermalization of Gauge Theories from Their Entanglement Spectrum, Phys. Rev. Lett. **129**, 011601 (2022).

[98] F. G. S. L. Brandão and M. J. Kastoryano, Finite correlation length implies efficient preparation of quantum thermal states, Commun. Math. Phys. **365**, 1 (2019).

[99] S. Lu, M. C. Bañuls, and J. I. Cirac, Algorithms for quantum simulation at finite energies, PRX Quantum **2**, 020321 (2021).

[100] M. Motta, C. Sun, A. T. Tan, M. J. O'Rourke, E. Ye, A. J. Minnich, F. G. Brandão, and G. K.-L. Chan, Determining eigenstates and thermal states on a quantum computer using quantum imaginary time evolution, Nat. Phys. **16**, 205 (2020).

[101] S.-N. Sun, M. Motta, R. N. Tazhigulov, A. T. K, Tan, Garnet Kin-Lic Chan, and A. J. Minnich, Quantum computation of finite-temperature static and dynamical properties of spin systems using quantum imaginary time evolution, PRX Quantum **2**, 010317 (2021).

[102] K. Temme, T. J. Osborne, K. G. Vollbrecht, D. Poulin, and F. Verstraete, Quantum metropolis sampling, Nature (London) **471**, 87 (2011).

[103] M. J. Kastoryano and F. G. Brandao, Quantum Gibbs samplers: The commuting case, Commun. Math. Phys. **344**, 915 (2016).

[104] M.-H. Yung and A. Aspuru-Guzik, A quantum–quantum Metropolis algorithm, Proc. Natl. Acad. Sci. U.S.A. **109**, 754 (2012).

[105] E. Bilgin and S. Boixo, Preparing Thermal States of Quantum Systems by Dimension Reduction, Phys. Rev. Lett. **105**, 170405 (2010).

[106] D. Poulin and P. Wocjan, Sampling from the Thermal Quantum Gibbs State and Evaluating Partition Functions with a Quantum Computer, Phys. Rev. Lett. **103**, 220502 (2009).

[107] A. Riera, C. Gogolin, and J. Eisert, Thermalization in Nature and on a Quantum Computer, Phys. Rev. Lett. **108**, 080402 (2012).

[108] D. Zhu, S. Johri, N. M. Linke, K. A. Landsman, C. Huerta Alderete, N. H. Nguyen, A. Y. Matsuura, T. H. Hsieh, and C. Monroe, Generation of thermofield double states and critical ground states with a quantum computer, Proc. Natl. Acad. Sci. U.S.A. **117**, 25402 (2020).

[109] A. N. Chowdhury and R. D. Somma, Quantum algorithms for Gibbs sampling and hitting-time estimation, Quantum Inf. Comput. **17**, 0041 (2017).

[110] B. M. Terhal and D. P. DiVincenzo, Problem of equilibration and the computation of correlation functions on a quantum computer, Phys. Rev. A **61**, 022301 (2000).

[111] H. Lamm and S. Lawrence, Simulation of Nonequilibrium Dynamics on a Quantum Computer, Phys. Rev. Lett. **121**, 170501 (2018).

[112] S. Harmalkar, H. Lamm, and S. Lawrence, Quantum simulation of field theories without state preparation, arXiv:2001.11490.

[113] G. Verdon, J. Marks, S. Nanda, S. Leichenauer, and J. Hidary, Quantum Hamiltonian-based models and the variational quantum thermalizer algorithm, arXiv:1910.02071.

[114] A. N. Chowdhury, G. H. Low, and N. Wiebe, A variational quantum algorithm for preparing quantum Gibbs states, arXiv:2002.00055.

[115] J. Wu and T. H. Hsieh, Variational Thermal Quantum Simulation via Thermofield Double States, Phys. Rev. Lett. **123**, 220502 (2019).

[116] R. Sagastizabal, S. Premaratne, B. Klaver, M. Rol, V. Negîrneac, M. Moreira, X. Zou, S. Johri, N. Muthusubramanian, M. Beekman *et al.*, Variational preparation of finite-temperature states on a quantum computer, npj Quantum Inf. **7**, 130 (2021).

[117] Y. Wang, G. Li, and X. Wang, Variational Quantum Gibbs State Preparation with a Truncated Taylor Series, Phys. Rev. Appl. **16**, 054035 (2021).

[118] N. Gomes, A. Mukherjee, F. Zhang, T. Iadecola, C.-Z. Wang, K.-M. Ho, P. P. Orth, and Y.-X. Yao, Adaptive variational quantum imaginary time evolution approach for ground state preparation, Adv. Quantum Technol. **4**, 2100114 (2021).

[119] A. Warren, L. Zhu, N. J. Mayhall, E. Barnes, and S. E. Economou, Adaptive variational algorithms for quantum Gibbs state preparation, arXiv:2203.12757.

[120] C. Jarzynski, Nonequilibrium Equality for Free Energy Differences, Phys. Rev. Lett. **78**, 2690 (1997).

[121] A. Schuckert, A. Bohrdt, E. Crane, and M. Knap, Probing finite-temperature observables in quantum simulators of spin systems with short-time dynamics, Phys. Rev. B **107**, L140410 (2023).

[122] L. Bassman, K. Klymko, D. Liu, N. M. Tubman, and W. A. de Jong, Computing free energies with fluctuation relations on quantum computers, arXiv:2103.09846.

[123] S. Sugiura and A. Shimizu, Canonical Thermal Pure Quantum State, Phys. Rev. Lett. **111**, 010401 (2013).

[124] S. Sugiura and A. Shimizu, Thermal Pure Quantum States at Finite Temperature, Phys. Rev. Lett. **108**, 240401 (2012).

[125] M. Hyuga, S. Sugiura, K. Sakai, and A. Shimizu, Thermal pure quantum states of many-particle systems, Phys. Rev. B **90**, 121110(R) (2014).

[126] C. Powers, L. Bassman Oftelie, D. Camps, and W. A. de Jong, Exploring finite temperature properties of materials with quantum computers, Sci. Rep. **13**, 1986 (2023).

[127] L. Coopmans, Y. Kikuchi, and M. Benedetti, Predicting Gibbs-state expectation values with pure thermal shadows, PRX Quantum **4**, 010305 (2023).

[128] See Supplemental Material at http://link.aps.org/supplemental/10.1103/PhysRevLett.131.081901 for additional background on TPQ states, performance comparisons between TPQ and PTPQ states, and discussions of confined phases of $\mathbb{Z}_2^{1+1}$, the Trotter error bound for imaginary time evolution presented in this Letter, impacts of link-operator conventions, and runtime scaling of the QITE algorithm, which includes Refs. [100,124,129–133].

[129] R. Kubo, Statistical mechanical theory of irreversible processes. 1. General theory and simple applications to magnetic and conduction problems, J. Phys. Soc. Jpn. **12**, 570 (1957).

[130] R. Somma, G. Ortiz, J. E. Gubernatis, E. Knill, and R. Laflamme, Simulating physical phenomena by quantum networks, Phys. Rev. A **65**, 042323 (2002).

[131] T. Iitaka and T. Ebisuzaki, Random phase vector for calculating the trace of a large matrix, Phys. Rev. E **69**, 057701 (2004).

[132] U. Borla, R. Verresen, F. Grusdt, and S. Moroz, Confined Phases of One-Dimensional Spinless Fermions Coupled to $Z_2$ Gauge Theory, Phys. Rev. Lett. **124**, 120503 (2020).

[133] S. Descombes and M. Thalhammer, An exact local error representation of exponential operator splitting methods for evolutionary problems and applications to linear Schrödinger equations in the semi-classical regime, BIT **50**, 729 (2010).

[134] P. Hauke, D. Marcos, M. Dalmonte, and P. Zoller, Quantum Simulation of a Lattice Schwinger Model in a Chain of Trapped Ions, Phys. Rev. X **3**, 041018 (2013).

[135] D. Banerjee, M. Bögli, M. Dalmonte, E. Rico, P. Stebler, U.-J. Wiese, and P. Zoller, Atomic Quantum Simulation of U(N) and SU(N) Non-Abelian Lattice Gauge Theories, Phys. Rev. Lett. **110**, 125303 (2013).

[136] D. Marcos, P. Rabl, E. Rico, and P. Zoller, Superconducting Circuits for Quantum Simulation of Dynamical Gauge Fields, Phys. Rev. Lett. **111**, 110504 (2013).

[137] J. C. Halimeh, H. Lang, J. Mildenberger, Z. Jiang, and P. Hauke, Gauge-symmetry protection using single-body terms, PRX Quantum **2**, 040311 (2021).

[138] M. Van Damme, J. Mildenberger, F. Grusdt, P. Hauke, and J. C. Halimeh, Suppressing nonperturbative gauge errors in the thermodynamic limit using local pseudogenerators, arXiv:2110.08041.

[139] E. Mathew and I. Raychowdhury, Protecting local and global symmetries in simulating $(1+1)$D non-Abelian gauge theories, Phys. Rev. D **106**, 054510 (2022).

[140] Y. S. Weinstein, W. G. Brown, and L. Viola, Parameters of pseudorandom quantum circuits, Phys. Rev. A **78**, 052332 (2008).

[141] J. Richter and A. Pal, Simulating Hydrodynamics on Noisy Intermediate-Scale Quantum Devices with Random Circuits, Phys. Rev. Lett. **126**, 230501 (2021).
[142] In addition to a small explicit breaking due to finite bare quark masses.
[143] J. Kogut, M. Stone, H. W. Wyld, J. Shigemitsu, S. H. Shenker, and D. K. Sinclair, Scales of Chiral Symmetry Breaking in Quantum Chromodynamics, Phys. Rev. Lett. **48**, 1140 (1982).
[144] E. Shuryak, Which chiral symmetry is restored in hot QCD?, Comments Nucl. Part. Phys. **21**, 235 (1994).
[145] S. Gottlieb, W. Liu, D. Toussaint, R. L. Renken, and R. L. Sugar, Estimating the Chiral-Symmetry–Restoration Temperature in Two-Flavor QCD, Phys. Rev. Lett. **59**, 1513 (1987).
[146] J. R. Morones-Ibarra, A. Enriquez-Perez-Gavilan, A. I. H. Rodriguez, F. V. Flores-Baez, N. B. Mata-Carrizalez, and E. V. Ordoñez, Chiral symmetry restoration and the critical end point in QCD, Open Phys. **15**, 1039 (2017).
[147] F. Karsch, Lattice QCD at high temperature and density, in *Lectures on Quark Matter* (Springer, New York, 2002), pp. 209–249.
[148] C. Hamer, J. Kogut, D. Crewther, and M. Mazzolini, The massive Schwinger model on a lattice: Background field, chiral symmetry and the string tension, Nucl. Phys. **B208**, 413 (1982).
[149] K. Melnikov and M. Weinstein, Lattice Schwinger model: Confinement, anomalies, chiral fermions, and all that, Phys. Rev. D **62**, 094504 (2000).
[150] J. Frank, E. Huffman, and S. Chandrasekharan, Emergence of Gauss' law in a $Z_2$ lattice gauge theory in $1+1$ dimensions, Phys. Lett. B **806**, 135484 (2020).
[151] H. Endo, C. Hotta, and A. Shimizu, From Linear to Nonlinear Responses of Thermal Pure Quantum States, Phys. Rev. Lett. **121**, 220601 (2018).
[152] M. Knap, A. Kantian, T. Giamarchi, I. Bloch, M. D. Lukin, and E. Demler, Probing Real-Space and Time-Resolved Correlation Functions with Many-Body Ramsey Interferometry, Phys. Rev. Lett. **111**, 147205 (2013).
[153] N. Y. Yao, F. Grusdt, B. Swingle, M. D. Lukin, D. M. Stamper-Kurn, J. E. Moore, and E. A. Demler, Interferometric approach to probing fast scrambling, arXiv: 1607.01801.
[154] F. Tonielli, N. Chakraborty, F. Grusdt, and J. Marino, Ramsey interferometry of non-Hermitian quantum impurities, Phys. Rev. Res. **2**, 032003(R) (2020).
[155] Qiskit contributors, Qiskit: An Open-source Framework for Quantum Computing (2021), 10.5281/zenodo .2573505.
[156] A. M. Childs, Y. Su, M. C. Tran, N. Wiebe, and S. Zhu, Theory of Trotter Error with Commutator Scaling, Phys. Rev. X **11**, 011020 (2021).
[157] R. M. Gingrich and C. P. Williams, Non-unitary probabilistic quantum computing, in *Proceedings of the Winter International Synposium on Information and Communication Technologies, WISICT '04* (Trinity College Dublin, Dublin, Ireland, 2004), pp. 1–6.
[158] F. Turro, A. Roggero, V. Amitrano, P. Luchi, K. A. Wendt, J. L. Dubois, S. Quaglioni, and F. Pederiva, Imaginary-time propagation on a quantum chip, Phys. Rev. A **105**, 022440 (2022).
[159] This may be called "unitary errors" if one were to perform real-time evolution.
[160] J. Emerson, Y. S. Weinstein, M. Saraceno, S. Lloyd, and D. G. Cory, Pseudo-random unitary operators for quantum information processing, Science **302**, 2098 (2003).
[161] R. Oliveira, O. C. O. Dahlsten, and M. B. Plenio, Generic entanglement Can Be Generated Efficiently, Phys. Rev. Lett. **98**, 130502 (2007).
[162] S. Boixo, S. V. Isakov, V. N. Smelyanskiy, R. Babbush, N. Ding, Z. Jiang, M. J. Bremner, J. M. Martinis, and H. Neven, Characterizing quantum supremacy in near-term devices, Nat. Phys. **14**, 595 (2018).
[163] Y. Nakata, C. Hirche, M. Koashi, and A. Winter, Efficient Quantum Pseudorandomness with Nearly Time-Independent Hamiltonian Dynamics, Phys. Rev. X **7**, 021006 (2017).
[164] S. McArdle, T. Jones, S. Endo, Y. Li, S. C. Benjamin, and X. Yuan, Variational ansatz-based quantum simulation of imaginary time evolution, npj Quantum Inf. **5**, 75 (2019).
[165] T. Jones, S. Endo, S. McArdle, X. Yuan, and S. C. Benjamin, Variational quantum algorithms for discovering Hamiltonian spectra, Phys. Rev. A **99**, 062304 (2019).
[166] T. d. L. Silva, M. M. Taddei, S. Carrazza, and L. Aolita, Fragmented imaginary-time evolution for early-stage quantum signal processors, arXiv:2110.13180.
[167] S.-H. Lin, R. Dilip, A. G. Green, A. Smith, and F. Pollmann, Real-and imaginary-time evolution with compressed quantum circuits, PRX Quantum **2**, 010342 (2021).
[168] R. Venugopalan, From glasma to quark–gluon plasma in heavy-ion collisions, J. Phys. G **35**, 104003 (2008).